INORGANIC CHEMISTRY FRONTIERS

RESEARCH ARTICLE

View Article Online
View Journal | View Issue

Check for updates

Cite this: *Inorg. Chem. Front.*, 2023, **10**, 6909

Luminescence detection of CH_2Cl_2 by varying Cu···Cu interactions in a flexible porous coordination polymer†

Wei-Jie Zhang,‡[a] Wan-Tao Chen,‡[a] Chen-Hui Li,[a] Wen-Zhu Sun,[a] Jia-Wen Ye,*[a] Ling Chen,*[a] Hai-Ping Wang*[a] and Xiao-Ming Chen[b]

Received 28th August 2023,
Accepted 8th October 2023

DOI: 10.1039/d3qi01723k

rsc.li/frontiers-inorganic

Owing to the weakness of the interaction between chlorohydrocarbon and the host framework, the development of reversible and vapochromic coordination polymer (CP)-based luminescence sensors for the detection of CH_2Cl_2 with a fast response is still challenging. In this study, a flexible Cu(I)-CP, $[Cu_2I_2(PPh_3)_2(PYZ)]$ (**CIPP**, PPh_3 = triphenylphosphine, PYZ = pyrazine) is reported. The intra-cluster Cu···Cu distance in **CIPP** is quite sensitive to the external stimuli, resulting in the corresponding luminescence color and intensity change. Based on this feature, the fast (11 s), distinguishing (wavelength shift of 45 nm), and reversible luminescence response of **CIPP** for CH_2Cl_2 is realized. Crystallographic analysis suggests that the presence/removal of CH_2Cl_2 can affect the Cu···Cu distance, which is the origin of the responsive luminescence. In addition, the multiple weak interactions between CH_2Cl_2 and the framework afford the strong adsorption of CH_2Cl_2 into **CIPP**, which can be maintained for at least 5 minutes when exposed to air, thereby ensuring accuracy in the sensing process.

Published on 10 October 2023. Downloaded on 2/16/2026 1:45:00 PM.

Introduction

Volatile organic compounds (VOCs) refer to organic compounds with high vapor pressure and low boiling point under ambient conditions, therefore, they have high volatility.[1,2] Long-term exposures to VOCs possibly cause damage to human health, such as damage to the liver, kidneys, and nervous system; thus the detection of VOCs is of critical significance.[3–5] Emitting units in porous coordination polymers (CPs) or metal–organic frameworks (MOFs) can interact with VOCs, leading to changes in the intensity or the wavelength of the luminescence. For example, by generating C–H···O or Cl···H interactions between the host and guest molecules, the luminescence detection of tetrahydrofuran (THF), *N*,*N*-dimethylformamide (DMF), dimethyl sulfoxide (DMSO), and CH_2Cl_2 can be realized.[6–8] In addition, the process of guest-adsorption/desorption in a porous CP is usually accompanied by the structural transformation, which further exhibits changes in the conformation or the charge transfer of the luminescent chromophore.[9,10]

Among VOCs, CH_2Cl_2 is widely used as a solvent or reagent not only in laboratories but also in a wide range of industrial applications, such as the production of paint removers, herbicides, and pesticides.[11] However, CH_2Cl_2 may cause damage to the liver and nervous system, and even potential carcinogenic effects.[12,13] Several methods have been developed for the detection of CH_2Cl_2, such as gas chromatography (GC)-mass spectrometry (GC-MS, 5 ng L^{-1}), gas chromatography-photo-ionization detectors (GC-PID, 1 ppm), and screen-printed electrodes (SPE, 17.3 μmol L^{-1}).[14–17] However, they display some shortcomings, such as the use of expensive instruments, tedious sample pretreatment processes, and the inability for *in situ* analysis. Compared to the above traditional ways, luminescence detection for VOCs based on porous CPs has unique advantages, such as fast response, visualization, and simplicity.[18–23] However, in comparison with usual VOCs, CH_2Cl_2 has difficulty forming strong interactions with the luminescent probes because of its low polarity and rather low boiling points. Therefore, reports about the luminescence response for CH_2Cl_2 in porous CPs and MOFs are rare.[8,24] Moreover, because of the weak interaction between CH_2Cl_2 and CPs, it is difficult for CH_2Cl_2 to directly affect the luminescent center in CPs and cause the solvatochromism/vapochromism. Generally, the reported luminescent CP sensors for

[a]*School of Biotechnology and Health Sciences, Wuyi University, Jiangmen, Guangdong 529000, PR China. E-mail: wyuchemyjw@126.com, wyuchemcling@126.com, wanghp@wyu.edu.cn*
[b]*MOE Key Laboratory of Bioinorganic and Synthetic Chemistry, School of Chemistry, Sun Yat-Sen University, Guangzhou 510275, PR China*

†Electronic supplementary information (ESI) available. CCDC 2258386, 2258387, 2258388 and 2258389. For ESI and crystallographic data in CIF or other electronic format see DOI: https://doi.org/10.1039/d3qi01723k

‡These authors contributed equally to this study.

Published on 10 October 2023. Downloaded on 2/16/2026 1:45:00 PM.

CH_2Cl_2 with fast response are based on the emission intensity change. It is rather difficult to design and prepare luminescent CPs with both chromatic and fast responses to CH_2Cl_2. Compared with the color-changeable luminescence detection, the intensity-depending method is more likely to cause errors due to test conditions and methods.[25–27]

Cu(I)-CPs have attracted much attention because of their low toxicity, low cost, and broad photophysical behaviors.[28–34] In particular, the intra-cluster Cu···Cu distance in copper clusters could be varied with external stimulus, resulting in changes in Cu···Cu interaction and corresponding emissions.[35,36] Based on this principle, we recently reported a series of Cu(I)-CPs with attractive optical properties, *i.e.*, long afterglow and multi-stimuli-responsive, properties, including thermochromism, mechanochromism, and solvatochromism/vapochromism.[37–40]

Herein, we report a Cu(I)-CP, $[Cu_2I_2(PPh_3)_2(PYZ)]$ (**CIPP**, PPh_3 = triphenylphosphine, PYZ = pyrazine), which has a flexible one-dimensional (1D) chain structure. **CIPP** displays different blue shifts in the luminescence after the adsorption of CH_2Cl_2, $CHCl_3$, and CH_3CN vapors. In order to investigate the vapochromic mechanism, **CIPP** with corresponding guests was also prepared. Detailed structural analyses show that compared to **CIPP**, the adsorption of guest molecules makes the Cu···Cu distances longer, resulting in luminescent blue shifts and higher emission energy. Meanwhile, **CIPP** exhibits fast response speed (11 s) and satisfactory reversibility. Furthermore, **CIPP** can retain CH_2Cl_2 for a long time, which is helpful for applications in the detection processes.

Results and discussion

Syntheses and characteristics

CIPP·CH_2Cl_2 (**CIPP-D**) was synthesized by the reaction of CuI, PPh_3, and PYZ in a CH_2Cl_2 solution. After drying under vacuum, the CH_2Cl_2 guest in **CIPP-D** was removed and the red **CIPP** crystals were obtained, referring to the reported method of a similar structure.[41] Single-crystal X-ray diffraction (SCXRD) demonstrates that **CIPP** belongs to the monoclinic *C*2/*c* space group. The crystallographic asymmetric unit of **CIPP** contains one and a half $[Cu_2(\mu\text{-}I)_2]$ clusters as nodes, a bridging bidentate PYZ, and three monodentate PPh_3 ligands, which directly coordinate with the copper ions (Fig. 1a). In contrast to the similar structure that has been reported,[42] there are two different clusters in **CIPP** with intra-cluster Cu···Cu distances of 2.7338(13) Å (Cu1···Cu1A) and 2.8557(16) Å (Cu2···Cu2), respectively (Fig. S1†). These two types of copper clusters are arranged at the ABAB intervals along the CP chain. The $[Cu_2(\mu\text{-}I)_2]$ clusters are interconnected by PYZ as a bridging ligand into the 1D chains (Fig. 1b). These 1D chains are stacked with each other to form the 3D structure *via* aromatic C–H···π interaction (Fig. 1c and S2†). Thermogravimetric (TG) analysis indicated that the **CIPP** was stable up to 115 °C, and no significant weight loss was observed before the collapse, proving that there was no guest molecule in the **CIPP** (Fig. S3†).

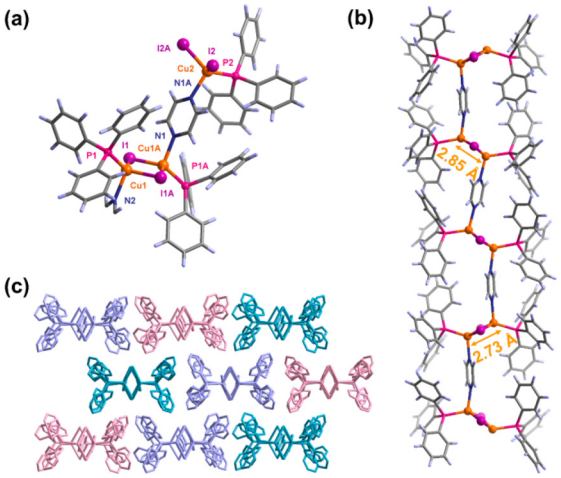

Fig. 1 (a) The asymmetric unit and (b) 1D chain of **CIPP**. Color codes: Cu, orange; I, purple; N, indigo; P, pink; C, gray; H, light purple. (c) The stacking mode between the chains of **CIPP**. Different colors are employed to distinguish separate chains. Hydrogen atoms are omitted for clarity.

Photophysical properties

UV–vis absorption and emission spectra of **CIPP** are shown in Fig. 2a. It shows the strong absorption from 200 to 600 nm, and the maximum absorption wavelength (λ_{abs}) was centered at approximately 427 nm, which can be assigned to the mixed metal-to-ligand charge transfer (MLCT) and halogen-to-ligand charge transfer (XLCT) transitions.[43] Because the Cu···Cu distance in **CIPP** is about 2.8 Å, the strong Cu(I)···Cu(I) interaction should be considered, which will affect the mixed MLCT/XLCT transition, and is usually accompanied by the longer wavelength emission. As observed under 365 nm excitation, **CIPP** shows orange-red luminescence with the maximum emission wavelength (λ_{em}) at 663 nm (Fig. S4†). This λ_{em} with rather low energy indicates the fairly large MLCT composition and strong Cu(I)···Cu(I) interaction. Meanwhile, the emissions of **CIPP** and **CIPP-D** do not change when varying the excited wavelength (260–460 nm), demonstrating the same emission center (Fig. S5†). Because the luminescence of Cu(I) clusters is reported to be sensitive to temperature, the emission spectra of **CIPP** at different temperatures were measured. As shown in Fig. 2b, from 80 K to 120 K, the emission of **CIPP** displayed both red-shifting and intensity-decreasing tendencies with increasing temperature, which agreed with the common thermal quenching (TQ) phenomenon.[44] However, when the the temperature was further increased, contrastingly, the emissions of **CIPP** showed blue shifts with the gradually enhanced intensity (Fig. 2c). Detailedly, the emission of **CIPP** shifted from 710 nm to 663 nm (120–300 K), which showed a significant wavelength shift of 47 nm (0.12 eV). Although some studies have promoted that such temperature-dependent luminescence in Cu(I) complexes may be caused by the "thermally activated delayed fluorescence" mechanism,[45,46] in this work, we tend to attribute this phenomenon to the slight

 This journal is © the Partner Organisations 2023

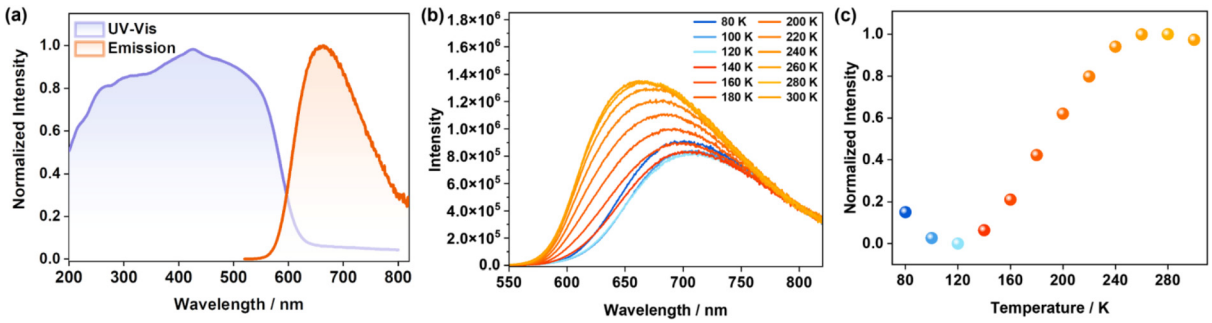

Fig. 2 (a) UV–vis absorption and emission spectra (excited at 365 nm) of **CIPP** in air at room temperature. (b) Temperature-dependent emission spectra of **CIPP**, from 80 K to 300 K, excited at 365 nm. (c) A scatter plot of the integral emission intensity of **CIPP** at the corresponding temperature, based on (b).

Published on 10 October 2023. Downloaded on 2/16/2026 1:45:00 PM.

lengthening of the Cu(I)···Cu(I) distance,[47,48] as the SCXRD measurements at variable temperatures further confirmed it (Fig. S6 and Table S1†). The increase in the Cu(I)···Cu(I) distance weakens the Cu···Cu interaction, resulting in the luminescent blue shift. Because the luminescence blue shifts from the near-infrared to the visible region, its non-radiative transition is reduced. Thus, besides the blue shift, it also exhibits luminescence intensity enhancement at the same time.

Interestingly, the obvious vapochromism of **CIPP** was observed (Fig. 3). Especially, when exposed to CH_2Cl_2 vapor, the luminescence of **CIPP** exhibited a distinct blueshift (45 nm), with the emission color change from orange-red (663 nm) to orange-yellow (618 nm). Moreover, other VOC vapors, such as CH_3CN and $CHCl_3$, can also result in similar blue shifts but with smaller changes (30 and 38 nm, respectively, Fig. 3a and c, respectively). When **CIPP** was exposed to other types of halohydrocarbon vapors, for example, CH_2Br_2, CH_2I_2, and $CHBr_3$, it exhibited similar luminescent vapochromism behavior, indicating that **CIPP** can detect the molecules with a similar size to CH_2Cl_2 (Fig. S7†). On the contrary,

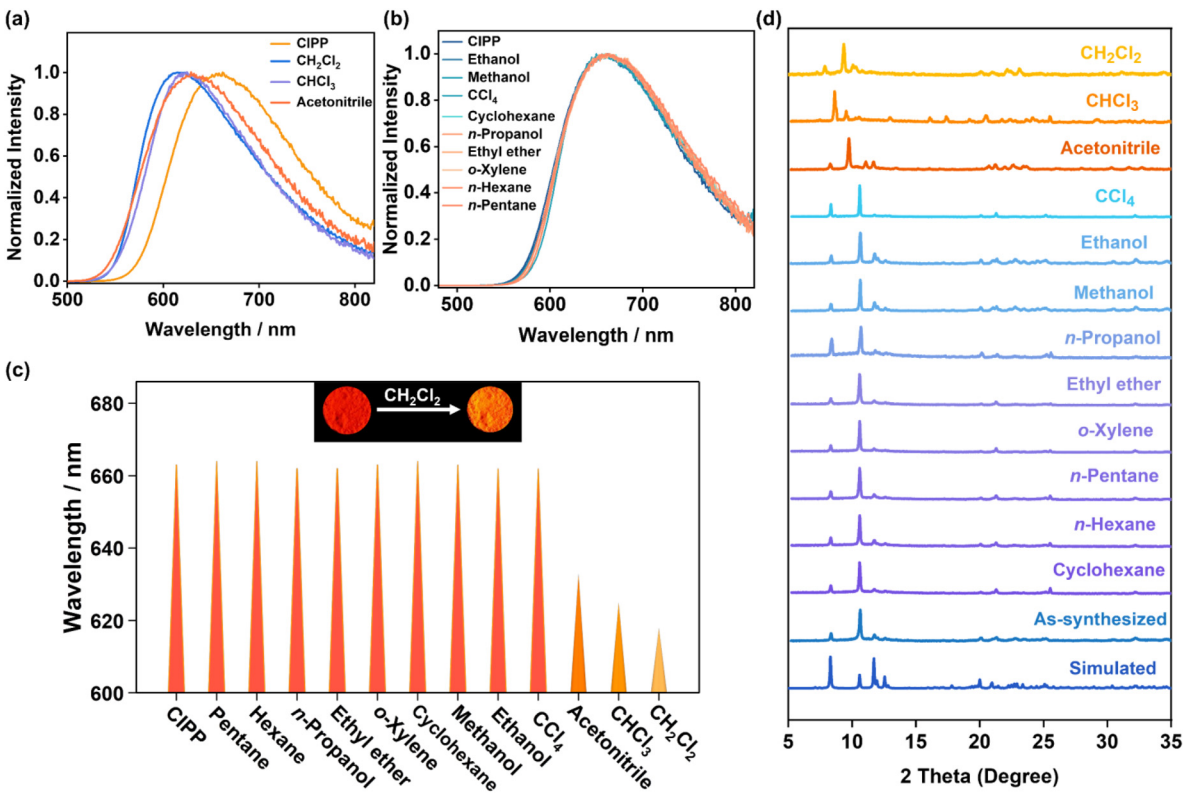

Fig. 3 Emission spectra of **CIPP** before and after exposure in (a) acetonitrile, CH_2Cl_2, $CHCl_3$ vapors, and (b) other VOCs. (c) The λ_{em} that was obtained from (a) and (b), excited at 365 nm. Insert: a photographs of **CIPP** before and after exposure in CH_2Cl_2, under 365 nm UV light. (d) PXRD patterns of **CIPP** before and after exposure in different VOCs.

Published on 10 October 2023. Downloaded on 2/16/2026 1:45:00 PM.

exposure to other common VOC vapors did not lead to the obvious luminescence variation for **CIPP** (Fig. 3b and c), which suggested the selective luminescence sensing and the potential application of halohydrocarbon and CH_3CN detection.

Mechanism of sensing for VOCs

Powder X-ray diffraction (PXRD) patterns were measured to reveal the structural transformation during the vapochromism. As shown in Fig. 3d, The PXRD results show that the structure of **CIPP** does not change after exposure to the most common VOC vapors, including CCl_4, ethanol, methanol, and cyclohexane, consistent with the corresponding irresponsive emission spectra shown in Fig. 3b and c. It is worth mentioning that the structure of **CIPP** in the gate-closing state is close-packed, making it difficult to adsorb these VOC molecules. The PXRD patterns in other VOC vapors, including CH_2Cl_2, $CHCl_3$, and CH_3CN, show remarkable changes (Fig. 3d). This means that these organic molecules are able to interact with **CIPP** by vapor diffusion, which opens the channels, illustrating the structural flexibility of **CIPP**. Such flexibility enables it to adsorb different molecules to form the structures in the opening state. The luminescence lifetimes of **CIPP** before and after exposure to VOC vapors are listed in Fig. S8,† which are all μs-scale and assigned to the phosphorescence.

To further clarify the structural transformations of **CIPP** in the vapochromic processes, the crystallographic structures of **CIPP** with different guest molecules were analyzed in detail, including **CIPP-D** (with CH_2Cl_2 guest), **CIPP-C** (with $CHCl_3$ guest), and **CIPP-A** (with acetonitrile guest), which crystallize from the corresponding organic solvents (Fig. S9†). The λ_{em} of the as-synthesized **CIPP-D** is almost the same as that of the fumigated **CIPP** powder in CH_2Cl_2 vapor. The comparison of the PXRD patterns of CH_2Cl_2-fumigated **CIPP** and **CIPP-D** indicates that the transformation from **CIPP** to **CIPP-D** is mostly complete (Fig. S10†). Meanwhile, the luminescence sensing is still sufficient by using only the surface of the compound, as the excitation light is difficult to deeply penetrate the crystals (Fig. S11†). The completed structural transformation was observed by directly immersing **CIPP** in CH_2Cl_2 solvent (Fig. S12†). Similar transformations for **CIPP** after exposure to $CHCl_3$ and CH_3CN can be also observed (Fig. S13 and S14†).

As shown in Fig. 4a and b, the molecular chains in **CIPP-D** are similar to those in guest-free **CIPP**, suggesting that they are not reconstructed after absorbing CH_2Cl_2. For **CIPP-D**, the gaps between molecular chains are filled with CH_2Cl_2 molecules, resulting in the expansion of the structure, which exhibits the flexibility of the crystal (Fig. 4b). Each CH_2Cl_2 molecule in **CIPP-D** is enclosed by four phenyl rings of PPh_3 and two PYZ ligands from the two adjacent chains (Fig. S15†). The chlorine atoms of the CH_2Cl_2 molecule point toward the pyrazine ligands of two adjacent chains. The dihedral angle between the pyrazine ligands of the two adjacent chains is *ca.* 25° and creates a void to accommodate a CH_2Cl_2 molecule (Fig. 4d). The chains of **CIPP-D** are also stacked by weak intermolecular interactions, such as those of **CIPP** (Fig. S16†). The structures in **CIPP-C** with $CHCl_3$ and **CIPP-A** with CH_3CN are

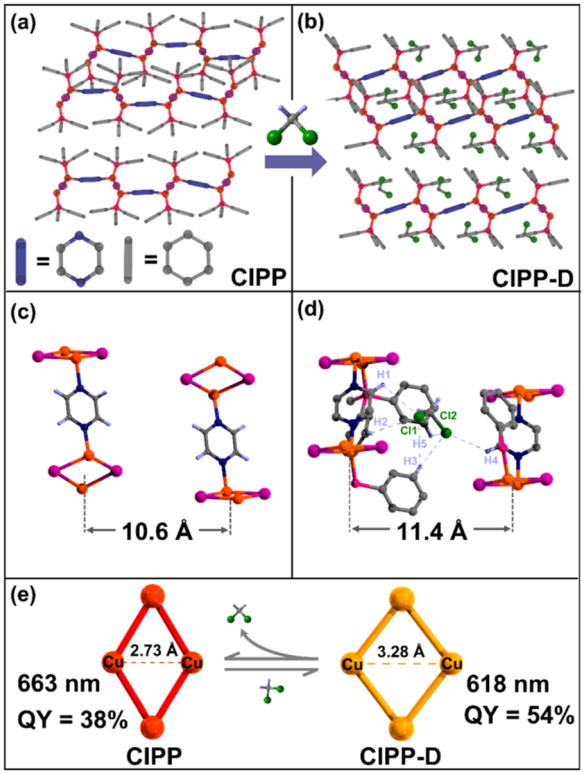

Fig. 4 Molecular chains stacking in (a) **CIPP** and (b) **CIPP-D** viewed along the *b*-axis, the purple cylinders represent the PYZ ligands and the gray ones are for the phenyl rings of PPh_3. The distance between adjacent molecular chains in (c) **CIPP** and (d) **CIPP-D**. Interactions in **CIPP-D**: Cl1···H1, 3.33 Å; Cl1···H2, 3.26 Å; Cl1···H3, 3.15 Å; Cl2···H3, 3.35 Å; Cl2···H4, 3.33 Å; Cl2···H5, 3.40 Å. (e) Cu···Cu distances of the $[Cu_2(\mu\text{-}I)_2]$ clusters in **CIPP** and **CIPP-D**. Color codes: Cu, orange; I, purple; Cl, green; N, indigo; P, pink; C, gray; H, light purple.

similar with those of **CIPP-D** (Fig. S17†). The CH_2Cl_2 molecules are ordered in the crystal structure and stabilized by multi-weak interactions with PYZ and PPh_3 ligands in the lattice (Fig. 4d and S18†). The closest distance between Cl atoms of CH_2Cl_2 and H atoms of triphenylphosphine is 3.08 Å, which shows the large tendency of Cl···H hydrophobic interaction. In addition, the closest C–H···π distance between CH_2Cl_2 and the aromatic ring is only 3.56 Å. In order to analyze the proportion of multi-weak interactions, Hirshfeld surfaces analysis was used (Fig. S19†).[49,50] The 2D fingerprint plots illustrated that the weak host–guest Cl···H interactions occupied a higher fraction (58.5%). The theoretical calculation demonstrated that the total binding energy between CH_2Cl_2 and **CIPP** framework is 85 kJ mol^{-1} (Table S2†). Meanwhile, the adjacent inter-chain distance in **CIPP-D** (11.44 Å) is markedly longer compared with that in **CIPP** (10.60 Å), due to the insertion of CH_2Cl_2 (Fig. 4c and d). Furthermore, the average occupancy area per chain for **CIPP-D** (31.2 $Å^2$) is also larger than that for **CIPP** (27.9 $Å^2$). Similarly, there is also a difference in the average occupancy areas of the molecular chains for **CIPP-C** (35.8 $Å^2$ per chain) and **CIPP-A** (30.3 $Å^2$ per chain), which are mainly dependent on the sizes of the guest molecules (Fig. S20†).

This journal is © the Partner Organisations 2023

Published on 10 October 2023. Downloaded on 2/16/2026 1:45:00 PM.

The intra-cluster Cu···Cu distance in **CIPP** is 2.73 Å, indicating a strong Cu···Cu interaction that leads to greatly reduced emission energy (1.87 eV). While for **CIPP-D**, with the lengthening of the inter-chain distance, $[Cu_2(\mu\text{-}I)_2]$ cluster stretches and the Cu···Cu distances increased to 3.28 Å, and 3.2378(8) Å for **CIPP-A** and 3.1479(7) Å for **CIPP-C** (Fig. S21†). For this reason, the intra-cluster Cu···Cu interaction in **CIPP-D** almost disappeared, thus it showed an obvious blueshift emission compared to that of **CIPP** (Fig. 4e). In addition, the increase of the Cu···Cu distance may enhance luminescence efficiency, as the photoluminescence quantum yields (PLQYs) are 38% for **CIPP**, and 54% for **CIPP-D** (Fig. 4e). This conclusion also explains why **CIPP** exhibits thermal luminescence enhancing phenomenon mentioned above, as the Cu···Cu distance in **CIPP** can slightly increase the warming process (120–298 K, Fig. S6†).

CH_2Cl_2 sensing properties

As **CIPP** shows the best sensing performance to CH_2Cl_2 with the greatest change of the luminescence among the VOCs, its responding performance to CH_2Cl_2 was analyzed in detail. First, when **CIPP** was exposed to the atmosphere of CH_2Cl_2 at different concentrations, it displayed a regularly changing tendency. As shown in Fig. 5, with the increase in CH_2Cl_2 concentration, the emission of **CIPP** gradually shifted from 663 nm to 618 nm. Moreover, a significant blueshift occurred at the CH_2Cl_2 concentration of 1 g L^{-1} (Fig. 5a), suggesting that the channel begins to open at this concentration.

The sensing speed and reversibility of **CIPP** were also tested by *in situ* experiments. The real-time continuous emission spectra were recorded using a charge-coupled device (CCD). CH_2Cl_2 molecules absorbed in **CIPP** could be removed by heating at 318 K, which was proved by both PXRD patterns and emission spectra (Fig. S22 and S23†). Therefore, to test the reversibility, **CIPP** powder was alternately placed in the atmosphere of saturated CH_2Cl_2 vapors at room temperature, and warm air without CH_2Cl_2 at 318 K. It should be noted that **CIPP** still showed a similar response to CH_2Cl_2 vapors after 16 cycles and the structure was maintained even after cyclic responses (Fig. 5b and S22†). As shown in Fig. 5d, in the saturated CH_2Cl_2 vapor, the luminescence of **CIPP** rapidly blue shifts within 11 s, suggesting a rather fast response. After the stabilization of the luminescence spectra, which suggested the saturation of CH_2Cl_2 absorption, CH_2Cl_2 from the sample was removed by blowing heated air (318 K), and the recovery time (back to the luminescence of **CIPP** phase) was about 66 s (Fig. 5e). The regenerated **CIPP-D** was able to maintain the emission without significant shift for about 5 min at room temperature (Fig. S24†), indicating that **CIPP** showed a relatively strong absorption of CH_2Cl_2, thus reducing the luminescence change in the measurement and improving the accuracy. In addition to CH_2Cl_2, the response time for $CHCl_3$ and

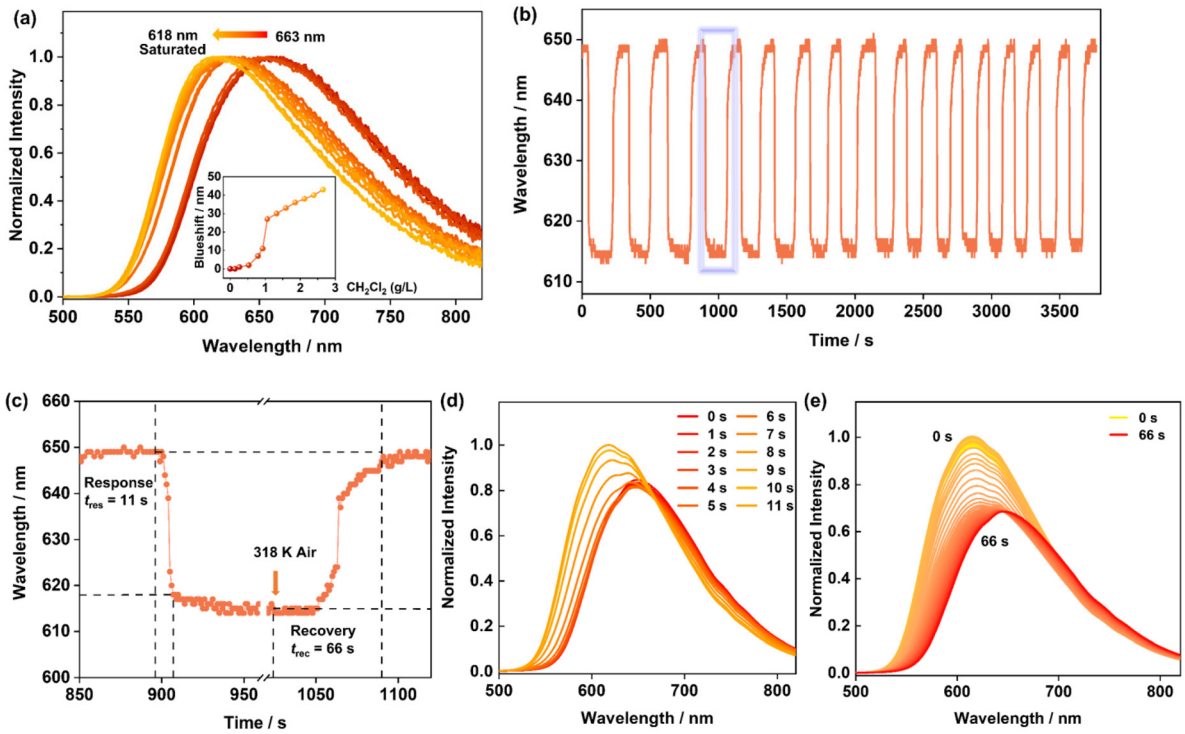

Fig. 5 (a) Emission spectra of **CIPP** in the atmosphere with various CH_2Cl_2 concentrations (0, 0.133, 0.265, 0.53, 0.795, 0.928, 1.06, 1.33, 1.59, 1.86, 2.12, 2.39, 2.65 g L^{-1}, from right to left) at room temperature. (b) The cyclic luminescence responses of **CIPP** under the alternation between saturated CH_2Cl_2 vapor and hot air (318 K). The vertical coordinate is the λ_{em} of the spectra per second. (c) Response curves in the range of purple square in (b) with a time range from 896 s to 907 s. (d) Time-dependent emission spectra of **CIPP** in saturated CH_2Cl_2 vapor, from 0 s to 11 s. (e) Time-dependent emission spectra of CH_2Cl_2-absorbed **CIPP** sample at 318 K, recorded once per second.

Published on 10 October 2023. Downloaded on 2/16/2026 1:45:00 PM.

CH_3CN vapors were also measured. For $CHCl_3$, the blue shift of λ_{em} was completed within 3 min (Fig. S25†). Such wavelength shift is smaller, and the response time is longer compared with that of the CH_2Cl_2 vapor. While for CH_3CN, the luminescence blueshift was completed within 60 s (Fig. S26†). The faster response speed for CH_2Cl_2 may be attributed to the rather high saturation vapor pressure of CH_2Cl_2 (46.5 kPa at 293 K), compared with those of $CHCl_3$ (21.28 kPa at 293 K) and CH_3CN (9.33 kPa at 293 K).[51,52]

Conclusions

A Cu(I)-CP named **CIPP** was synthesized and characterized extensively. **CIPP** displayed luminescence vapochromic response to CH_2Cl_2, $CHCl_3$, and CH_3CN vapors. Benefitting from the flexibility of **CIPP**, the intra-cluster Cu···Cu distance varies when it absorbs guest molecules and transforms into the gate-opening state. Especially, the interaction with CH_2Cl_2 allows **CIPP** to display a remarkable luminescence wavelength for the blue shift (45 nm). Moreover, **CIPP** exhibits fast luminescence color variation (*ca.* 11 s) and excellent reversibility for sensing CH_2Cl_2. Due to the multi-weak interactions, **CIPP** can hold CH_2Cl_2 for 5 minutes at room temperature in air.

Experimental

All the chemicals were obtained from commercial sources and used as received without further purification unless otherwise noted. Powder X-ray diffraction (PXRD) patterns were recorded on a Rigaku Mini diffractometer with Cu-Kα (λ = 1.54184 Å) radiation. UV-vis absorption spectra were recorded on a Shimadzu UV-3600i Plus UV-VIS-NIR absorption spectrometer. Thermogravimetric (TG) analyses were performed on a METTLER TOLEDO TGA/DSC 3+ instrument with a ramping rate of 10.0 °C min^{-1} under a nitrogen atmosphere. Elemental analysis (C, H, and N) was performed on an Elementar Vario EL Cube.

Preparation

For **CIPP-D** and **CIPP**: PYZ (16 mg, 0.2 mmol) and PPh_3 (105 mg, 0.40 mmol) were completely dissolved in dichloromethane (5 mL), followed by the addition of CuI (76 mg, 0.4 mmol) at room temperature. The orange **CIPP-D** crystals were formed from the transparent liquid after about 7 hours. The crystals were filtered and washed with CH_2Cl_2, then dried under vacuum to obtain orange-red **CIPP** crystals (yield = 60%). Elemental analysis calcd for $C_{20}H_{17}CuINP$ (**CIPP**): C, 48.75; H, 3.48; N, 2.84. Found: C, 48.80; H, 3.83; N, 2.64.

For **CIPP-A**: **CIPP-A** was synthesized by a similar method to that of **CIPP-D** by replacing the CH_2Cl_2 solvent with the CH_3CN solvent (yield = 54%).

For **CIPP-C**: PYZ (32 mg, 0.4 mmol) and PPh_3 (105 mg, 0.40 mmol) were completely dissolved in $CHCl_3$ (5 mL) at 278 K, followed by the addition of CuI (76 mg, 0.4 mmol). Then, the solution was kept at 278 K for about one day, and orange **CIPP-C** crystals were observed. The crystals were filtered and washed with cold $CHCl_3$ (yield = 47%). Among these, **CIPP-A** was reported in the previous literature.[36]

Single-crystal X-ray diffraction

Diffraction data were collected on a Rigaku XtaLAB single-crystal diffractometer by using Cu-Kα radiation (λ = 1.54184 Å). The structures were solved using the direct methods and refined with the full-matrix least-squares method on F^2 using the SHELXTL package.[53] Anisotropic thermal parameters were used to refine all non-hydrogen atoms. All hydrogen atoms were generated geometrically. Crystallographic data and details of data collection and refinements are summarized in Table S1.† CCDC 2258386 (**CIPP**), 2258387 (**CIPP-D**), 2258388 (**CIPP-C**), and 2258389 (**CIPP-150K**) contain supplementary crystallographic data for this work.†

Photoluminescence measurement

Photoluminescence measurements were performed on an Edinburgh FLS1000 fluorescence spectrometer. The emission spectra were recorded on the spectrometer equipped with a continuous Xe lamp. The luminescence decay experiments were performed on the same spectrometer equipped with a variable pulsed laser (VPL) at 375 ± 10 nm as the excitation source. The temperature was controlled using an Oxford temperature controller. The photoluminescence quantum yields (PLQYs) were measured on the same spectrometer in the integrating sphere.

The *in situ* experiment was recorded using an Ocean QE Pro charge-coupled device (CCD) equipped with a 365 nm LED. Real-time sensing of CH_2Cl_2 was realized using CH_2Cl_2 liquid to provide the saturated vapor under ambient conditions. After removing CH_2Cl_2 using hot air at 318 K, **CIPP** was cooled to room temperature by blowing normal air (detected by thermometer).

Conflicts of interest

There are no conflicts to declare.

Acknowledgements

We gratefully acknowledge the financial support of the National Natural Science Foundation of China (22101211, 21901189), Municipal Science and Technology Bureau (Jiangke 2021-76), MOE Key Laboratory of Bioinorganic and Synthetic Chemistry (BISC2022A04), Scientific Research Ability Improvement Project of Key Discipline Construction from the Education Department of Guangdong Province (2022ZDJS027), and the NSF of Guangdong Province (2017A030310258).

 This journal is © the Partner Organisations 2023

Published on 10 October 2023. Downloaded on 2/16/2026 1:45:00 PM.

References

1 Y. Shen, A. Tissot and C. Serre, Recent progress on MOF-based optical sensors for VOC sensing, *Chem. Sci.*, 2022, **13**, 13978–14007.
2 H. Y. Li, S. N. Zhao, S. Q. Zang and J. Li, Functional metal–organic frameworks as effective sensors of gases and volatile compounds, *Chem. Soc. Rev.*, 2020, **49**, 6364–6401.
3 S. Joshi, The Sick Building Syndrome, *Indian J. Occup. Health*, 2008, **12**, 61–64.
4 H. Ibrahim, S. Moru, P. Schnable and L. Dong, Wearable Plant Sensor for In Situ Monitoring of Volatile Organic Compound Emissions from Crops, *ACS Sens.*, 2022, **7**, 2293–2302.
5 D. S. Li, B. Y. Zhu, K. Pang, Q. Zhang, M. J. Qu, W. T. Liu, Y. Q. Fu and J. Xie, Virtual Sensor Array Based on Piezoelectric Cantilever Resonator for Identification of Volatile Organic Compounds, *ACS Sens.*, 2022, **7**, 1555–1563.
6 J. J. Pang, Z. Q. Yao, K. Zhang, Q. W. Li, Z. X. Fu, R. Zheng, W. Li, J. Xu and X. H. Bu, Real-Time In Situ Volatile Organic Compound Sensing by a Dual-Emissive Polynuclear Ln-MOF with Pronounced Ln(III) Luminescence Response, *Angew. Chem., Int. Ed.*, 2023, **62**, e202217456.
7 Z. Q. Yao, K. Wang, R. Liu, Y. J. Yuan, J. J. Pang, Q. W. Li, T. Y. Shao, Z. G. Li, R. Feng, B. Zou, W. Li, J. Xu and X. H. Bu, Dynamic Full-Color Tuning of Organic Chromophore in a Multi-Stimuli-Responsive 2D Flexible MOF, *Angew. Chem., Int. Ed.*, 2022, **61**, e202202073.
8 C. Y. Liu, X. R. Chen, H. X. Chen, Z. Niu, H. Hirao, P. Braunstein and J. P. Lang, Ultrafast Luminescent Light-Up Guest Detection Based on the Lock of the Host Molecular Vibration, *J. Am. Chem. Soc.*, 2020, **142**, 6690–6697.
9 X. Y. Dong, H. L. Huang, J. Y. Wang, H. Y. Li and S. Q. Zang, A Flexible Fluorescent SCC-MOF for Switchable Molecule Identification and Temperature Display, *Chem. Mater.*, 2018, **30**, 2160–2167.
10 L. Chen, J. W. Ye, H. P. Wang, M. Pan, S. Y. Yin, Z. W. Wei, L. Y. Zhang, K. Wu, Y. N. Fan and C. Y. Su, Ultrafast water sensing and thermal imaging by a metal–organic framework with switchable luminescence, *Nat. Commun.*, 2017, **8**, 15985.
11 World Health Organization and International Agency for Research on Cancer, Dichloromethane, *IARC Monogr. Eval. Carcinog. Risks Hum.*, 1999, **71**(Part 1), 251–315.
12 A. Hoang, K. Fagan, D. L. Cannon, S. D. G. Rayasam, R. Harrison, D. Shusterman and V. Singla, Assessment of Methylene Chloride-Related Fatalities in the United States, 1980-2018, *JAMA Intern. Med.*, 2021, **181**, 797–805.
13 P. M. Schlosser, A. S. Bale, C. F. Gibbons, A. Wilkins and G. S. Cooper, Human health effects of dichloromethane: key findings and scientific issues, *Environ. Health Perspect.*, 2015, **123**, 114–119.
14 I. Ueta, S. Kamei and Y. Saito, Needle extraction device for rapid and quantitative gas chromatographic determination of volatile chlorinated hydrocarbons and benzene in soil, *J. Chromatogr. A*, 2022, **1685**, 463586.
15 T. Sakai, Y. Morita and C. Wakui, Biological monitoring of workers exposed to dichloromethane, using head-space gas chromatography, *J. Chromatogr. B: Anal. Technol. Biomed. Life Sci.*, 2002, **778**, 245–250.
16 E.-B. Kim, Abdullah, S. Ameen, M. S. Akhtar and H. S. Shin, Environment-friendly and highly sensitive dichloromethane chemical sensor fabricated with ZnO nanopyramids-modified electrode, *J. Taiwan Inst. Chem. Eng.*, 2019, **102**, 143–152.
17 D. Poli, P. Manini, R. Andreoli, I. Franchini and A. Mutti, Determination of dichloromethane, trichloroethylene and perchloroethylene in urine samples by headspace solid phase microextraction gas chromatography-mass spectrometry, *J. Chromatogr. B: Anal. Technol. Biomed. Life Sci.*, 2005, **820**, 95–102.
18 J. R. Askim, M. Mahmoudi and K. S. Suslick, Optical sensor arrays for chemical sensing: the optoelectronic nose, *Chem. Soc. Rev.*, 2013, **42**, 8649–8682.
19 F. P. Yang, Q. T. He, H. Jiang, Z. Li, W. Chen, R. L. Chen, X. Y. Tang, Y. P. Cai and X. J. Hong, Rapid and Specific Enhanced Luminescent Switch of Aniline Gas by MOFs Assembled from a Planar Binuclear Cadmium(II) Metalloligand, *Inorg. Chem.*, 2022, **61**, 10844–10851.
20 I. S. Krytchankou, I. O. Koshevoy, V. V. Gurzhiy, V. A. Pomogaev and S. P. Tunik, Luminescence Solvato- and Vapochromism of Alkynyl-Phosphine Copper Clusters, *Inorg. Chem.*, 2015, **54**, 8288–8297.
21 R. W. Huang, Y. S. Wei, X. Y. Dong, X. H. Wu, C. X. Du, S. Q. Zang and T. C. W. Mak, Hypersensitive dual-function luminescence switching of a silver-chalcogenolate cluster-based metal–organic framework, *Nat. Chem.*, 2017, **9**, 689–697.
22 W. M. He, Z. Zhou, Z. Han, S. Li, Z. Zhou, L. F. Ma and S. Q. Zang, Ultrafast Size Expansion and Turn-On Luminescence of Atomically Precise Silver Clusters by Hydrogen Sulfide, *Angew. Chem., Int. Ed.*, 2021, **60**, 8505–8509.
23 Y. Yu, J. P. Ma, C. W. Zhao, J. Yang, X. M. Zhang, Q. K. Liu and Y. B. Dong, Copper(I) Metal–Organic Framework: Visual Sensor for Detecting Small Polar Aliphatic Volatile Organic Compounds, *Inorg. Chem.*, 2015, **54**, 11590–11592.
24 L. Guan, Z. Jiang, Y. Cui, Y. Yang, D. Yang and G. Qian, An MOF-Based Luminescent Sensor Array for Pattern Recognition and Quantification of Metal Ions, *Adv. Opt. Mater.*, 2021, **9**, 2002180.
25 Z. Han, Y. Si, X. Y. Dong, J. H. Hu, C. Zhang, X. H. Zhao, J. W. Yuan, Y. Wang and S. Q. Zang, Smart Reversible Transformations between Chiral Superstructures of Copper Clusters for Optical and Chiroptical Switching, *J. Am. Chem. Soc.*, 2023, **145**, 6166–6176.
26 W. Cao, T. Xia, Y. Cui, Y. Yu and G. Qian, Lanthanide metal–organic frameworks with nitrogen functional sites for the highly selective and sensitive detection of NADPH, *Chem. Commun.*, 2020, **56**, 10851–10854.

Published on 10 October 2023. Downloaded on 2/16/2026 1:45:00 PM.

27 J. Wang, D. Li, Y. Ye, Y. Qiu, J. Liu, L. Huang, B. Liang and B. Chen, A Fluorescent Metal–Organic Framework for Food Real-Time Visual Monitoring, *Adv. Mater.*, 2021, **33**, 2008020.
28 J. Troyano, F. Zamora and S. Delgado, Copper(I)–iodide cluster structures as functional and processable platform materials, *Chem. Soc. Rev.*, 2021, **50**, 4606–4628.
29 X. Hei, W. Liu, K. Zhu, S. J. Teat, S. Jensen, M. Li, D. M. O'Carroll, K. Wei, K. Tan, M. Cotlet, T. Thonhauser and J. Li, Blending Ionic and Coordinate Bonds in Hybrid Semiconductor Materials: A General Approach toward Robust and Solution-Processable Covalent/Coordinate Network Structures, *J. Am. Chem. Soc.*, 2020, **142**, 4242–4253.
30 J. P. Zobel, A. M. Wernbacher and L. González, Efficient Reverse Intersystem Crossing in Carbene-Copper-Amide TADF Emitters via an Intermediate Triplet State, *Angew. Chem., Int. Ed.*, 2023, **62**, e202217620.
31 J. J. Wang, C. Chen, W. G. Chen, J. S. Yao, J. N. Yang, K. H. Wang, Y. C. Yin, M. M. Yao, L. Z. Feng, C. Ma, F. J. Fan and H. B. Yao, Highly Luminescent Copper Iodide Cluster Based Inks with Photoluminescence Quantum Efficiency Exceeding 98%, *J. Am. Chem. Soc.*, 2020, **142**, 3686–3690.
32 B. L. Han, Z. Liu, L. Feng, Z. Wang, R. K. Gupta, C. M. Aikens, C. H. Tung and D. Sun, Polymorphism in Atomically Precise Cu_{23} Nanocluster Incorporating Tetrahedral $[Cu_4]^0$ Kernel, *J. Am. Chem. Soc.*, 2020, **142**, 5834–5841.
33 P. P. Sun, B. L. Han, H. G. Li, C. K. Zhang, X. Xin, J. M. Dou, Z. Y. Gao and D. Sun, Real-Time Fluorescent Monitoring of Kinetically Controlled Supramolecular Self-Assembly of Atom-Precise Cu8 Nanocluster, *Angew. Chem., Int. Ed.*, 2022, **61**, e202200180.
34 C. Zhang, Z. Wang, W. D. Si, L. Wang, J. M. Dou, Z. Y. Gao, C. H. Tung and D. Sun, Solvent-Induced Isomeric Cu_{13} Nanoclusters: Chlorine to Copper Charge Transfer Boosting Molecular Oxygen Activation in Sulfide Selective Oxidation, *ACS Nano*, 2022, **16**, 9598–9607.
35 J. Conesa-Egea, F. Zamora and P. Amo-Ochoa, Perspectives of the smart Cu-Iodine coordination polymers: A portage to the world of new nanomaterials and composites, *Coord. Chem. Rev.*, 2019, **381**, 65–78.
36 Q. Benito, X. F. Le Goff, S. Maron, A. Fargues, A. Garcia, C. Martineau, F. Taulelle, S. Kahlal, T. Gacoin, J. P. Boilot and S. Perruchas, Polymorphic Copper Iodide Clusters: Insights into the Mechanochromic Luminescence Properties, *J. Am. Chem. Soc.*, 2014, **136**, 11311–11320.
37 L. Chen, X. B. Dong, H. Y. Liao, W. J. Zhang, Z. W. Mo, H. P. Wang, J. W. Ye and X. M. Chen, Long-Range Rigidity Induced Ultralong Cluster-Centered Phosphorescence, *Chem. Mater.*, 2022, **34**, 9182–9189.
38 L. Chen, X. B. Dong, Z. W. Mo, H. P. Wang, J. W. Ye, K. Zhang and X. M. Chen, Efficient Restraint of Intra-Cluster Aggregation-Caused Quenching Effect Lighting Room-Temperature Photoluminescence, *Adv. Opt. Mater.*, 2021, **9**, 2100757.
39 W. T. Chen, L. Chen, Z. Y. Liang, Z. W. Mo, J. W. Ye and X. M. Chen, Multiple Flexibilities Trigger Luminescent Piezochromism of Closely Packed Cu(I) Coordination Polymers, *Adv. Opt. Mater.*, 2023, **11**, 2202771.
40 W. T. Chen, C. H. Li, W. Q. Zhou, J. T. Huang, J. W. Ye and L. Chen, A One-Dimensional Cu(I) Coordination Polymer with Optical Sensing of Oxygen and Temperature, *Inorganics*, 2022, **10**, 253.
41 H. Araki, K. Tsuge, Y. Sasaki, S. Ishizaka and N. Kitamura, Luminescence ranging from red to blue: a series of copper (I)-halide complexes having rhombic $\{Cu_2(\mu\text{-}X)_2\}$ (X = Br and I) units with N-heteroaromatic ligands, *Inorg. Chem.*, 2005, **44**, 9667–9675.
42 M. Henary, J. L. Wootton, S. I. Khan and J. I. Zink, Structure and Assignment of the Luminescence of a New Mixed-Ligand Copper(I) Polymer, *Inorg. Chem.*, 1997, **36**, 796–801.
43 S. Perruchas, C. Tard, X. F. Le Goff, A. Fargues, A. Garcia, S. Kahlal, J. Y. Saillard, T. Gacoin and J. P. Boilot, Thermochromic Luminescence of Copper Iodide Clusters: The Case of Phosphine Ligands, *Inorg. Chem.*, 2011, **50**, 10682–10692.
44 Y. H. Kim, P. Arunkumar, B. Y. Kim, S. Unithrattil, E. Kim, S. H. Moon, J. Y. Hyun, K. H. Kim, D. Lee, J. S. Lee and W. B. Im, A zero-thermal-quenching phosphor, *Nat. Mater.*, 2017, **16**, 543–550.
45 H. Yersin, R. Czerwieniec, M. Z. Shafikov and A. F. Suleymanova, TADF Material Design: Photophysical Background and Case Studies Focusing on CuIand AgIComplexes, *ChemPhysChem*, 2017, **18**, 3508–3535.
46 M. El Sayed Moussa, S. Evariste, H. L. Wong, L. Le Bras, C. Roiland, L. Le Polles, B. Le Guennic, K. Costuas, V. W. W. Yam and C. Lescop, A solid state highly emissive Cu(i) metallacycle: promotion of cuprophilic interactions at the excited states, *Chem. Commun.*, 2016, **52**, 11370–11373.
47 T. H. Kim, Y. W. Shin, J. H. Jung, J. S. Kim and J. Kim, Crystal-to-Crystal Transformation between Three CuI Coordination Polymers and Structural Evidence for Luminescence Thermochromism, *Angew. Chem., Int. Ed.*, 2008, **47**, 685–688.
48 D. Sun, S. Yuan, H. Wang, H. F. Lu, S. Y. Feng and D. F. Sun, Luminescence thermochromism of two entangled copper-iodide networks with a large temperature-dependent emission shift, *Chem. Commun.*, 2013, **49**, 6152–6154.
49 F. F. Gao, H. Song, Z. G. Li, Y. Qin, X. Li, Z. Q. Yao, J. H. Fan, X. Wu, W. Li and X. H. Bu, Pressure-Tuned Multicolor Emission of 2D Lead Halide Perovskites with Ultrahigh Color Purity, *Angew. Chem., Int. Ed.*, 2023, **62**, e202218675.
50 P. R. Spackman, M. J. Turner, J. J. McKinnon, S. K. Wolff, D. J. Grimwood, D. Jayatilaka and M. A. Spackman, CrystalExplorer: a program for Hirshfeld surface analysis, visualization and quantitative analysis of molecular crystals, *J. Appl. Crystallogr.*, 2021, **54**, 1006–1011.

 This journal is © the Partner Organisations 2023

51 Y. Tian, H. Ding, Q. Jiao and Y. Shi, Influence of Solvents on the Formation of Honeycomb Films by Water Droplets Templating, *Macromol. Chem. Phys.*, 2006, **207**, 545–553.
52 N. P. Lebedeva and L. Boon-Brett, Considerations on the Chemical Toxicity of Contemporary Li-Ion Battery Electrolytes and Their Components, *J. Electrochem. Soc.*, 2016, **163**, A821–A830.
53 G. M. Sheldrick, SHELXT– Integrated space-group and crystal-structure determination, *Acta Crystallogr., Sect. A: Found. Adv.*, 2015, **71**, 3–8.

Published on 10 October 2023. Downloaded on 2/16/2026 1:45:00 PM.